CZECH TECHNICAL UNIVERSITY IN PRAGUE

FACULTY OF ELECTRICAL ENGINEERING

GRADUATE THESIS

2022

IVAN GRINIKOV

MASTER‘S THESIS ASSIGNMENT

I. Personal and study details

Student's name: **Grinikov Ivan** Personal ID number: **511414**

Faculty / Institute: **Faculty of Electrical Engineering**

Department / Institute: **Department of Economics, Management and Humanities**

Study program: **Electrical Engineering, Power Engineering and Management**

Specialisation: **Management of Power Engineering and Electrotechnics**

II. Master’s thesis details

Master’s thesis title in English:

Economical efficiency of energy storage into hydrogen using a tungsten carbide catalyst

Master’s thesis title in Czech:

Ekonomická efektivnost ukládání energie do vodíku pomocí katalyzátoru z karbidu wolframu

Guidelines:

1. Energy storage methods - literature search
2. Estimation of CAPEX and OPEX of selected energy storage modes including a hydrogen accumulation option using a tungsten carbide catalyst
3. Comparison of the selected variants with the P2H variant using a tungsten carbide catalyst
4. Sensitivity analysis of recomended solution

Bibliography / sources:

RICHARD A. BREALEY, .. STEWART C. MYERS, .. FRANKLIN ALLEN, .., Richard A. Brealey, .. Stewart C. Myers, .. Franklin Allen, .. Principles of corporate finance. 9th ed. [international edition]. Boston, Mass: McGraw-Hill, 2008. ISBN 00-712-6675-5.
M. Aneke, M. Wang: Energy storage technologies and real life applications – A state of the art. review. Applied Energy 179 (2016) 350–377, Elsevier, London.

Name and workplace of master’s thesis supervisor:

Ing. Miroslav Vítek, CSc. 13116

Name and workplace of second master’s thesis supervisor or consultant:

Date of master’s thesis assignment: **16.02.2022** Deadline for master's thesis submission: **20.05.2022**

Assignment valid until: **19.02.2024**

Ing. Miroslav Vítek, CSc. Supervisor’s signature	Head of department’s signature	prof. Mgr. Petr Páta, Ph.D. Dean’s signature

III. Assignment receipt

The student acknowledges that the master’s thesis is an individual work. The student must produce his thesis without the assistance of others, with the exception of provided consultations. Within the master’s thesis, the author must state the names of consultants and include a list of references.

Date of assignment receipt	Student’s signature

Declaration: *I hereby declare that this master's thesis is the product of my own independent work and that I have clearly stated all information sources used in the thesis according to Methodological Instruction No. 1/2009 – "On maintaining ethical principles when working on a university final project, CTU in Prague".*

Date: *Signature:*

Abstract: In this thesis, cubic tungsten carbide was studied: methods of its synthesis (possible and used), its application in energy storage through electrolysis, other possible ways of energy storage, as well as the economic efficiency of these technologies. Unfortunately, cubic tungsten carbide at this stage of development proved to be economically inefficient: the gain in capital investments does not offset the increase in operating costs. The material needs further study and development. Sensitivity analysis of electrolysis and methane reforming steam was also performed. For electrolysis, efficiency remains a key parameter. In the past (2018), a significant increase in the cost of gas was required in order for the production of green hydrogen to be cost-effective. At the moment (2022) economically viable production of hydrogen through electrolysis looks possible

Content

List of abbreviations

CAPEX	capital expenditures
CB	circuit breaker
CC	coaxial cable
CCCP	charging current control panel
CE	counter electrode
CES	capacitive energy storage
CM	collector module
CMPA	coaxial magnetic plasma accelerator
COS	cut-off switch
CP	control panel
CRU	charging resistor unit
CS	control system
DC	discharge control
EI	electromagnetic interlock
HER	hydrogen evolution reaction
HVR	high voltage rectifier
HVT	high voltage transformer
ICU	ignitron control unit
ISG	ignitron spark gap
LSV	linear sweep voltammetry
MSU	magnetic starter unit
OPEX	operating expenditures
PD	potential divider
PG	pulse generator
PL	power lead of CP
PLS	position limit switch
PR	pulling relay
PT	pulsing transformer
RE	reference electrode
SC	short circuit (control)
SEM	scanning electron microscopy
SL	signal lamp
TEM	transmission electron microscopy
WE	working electrode
XRD	x-ray diffractometry

Introduction

In the modern world, the problem of CO_2 emission is relevant. The world is gradually phasing out the use of fossil fuels, so the need for environmentally friendly fuels is increasing.

One of the fuels could be green hydrogen. At the moment, the cheapest way to produce hydrogen is steam methane reforming. For such a process, natural gas is needed, and subsequently carbon dioxide is released, hydrogen is not considered environmentally friendly.

The most efficient way to produce green hydrogen is polymer electrolyte membrane electrolysis (PEM). However, to achieve high efficiency, many additional parts are used, which increases capital costs.

Membraneless electrolysis is not as efficient, so its commercial use is not widespread. However, the design is simple and capital costs are low, making membraneless electrolysis a promising technology (figure 1).

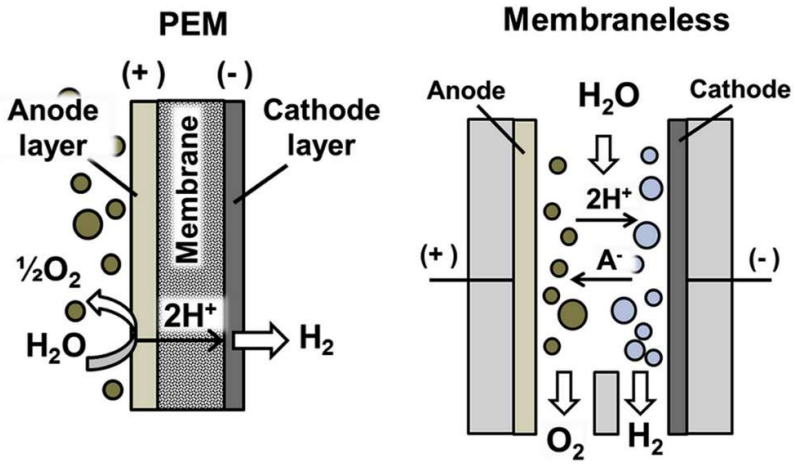

Figure 1 – Simplified schemes of PEM and membraneless electrolysis [1]

Both types of electrolysis require expensive electrodes with platinum group catalysts. For PEM, the relative cost of electrodes is low, but for membraneless electrolyzers, the price ratio is higher.

It is possible to considerably reduce the capital cost of platinum electrodes for membraneless electrodes by using other, cheaper materials. One such material could be cubic tungsten carbide: a material with electrocatalytic properties, which components (tungsten and carbon) are much cheaper than platinum.

This modification of tungsten carbide known relatively recently is not as common as hexagonal tungsten carbide. At the moment, there is no commercially viable way to produce it, that is why synthesis of it is open task for present science.

Plasma-dynamic synthesis with high temperatures and rapid cooling with ultra-fast plasma jets was used in production of the cubic tungsten carbide in this work: material with some properties was obtain and studying its implementation is the aim of this work.

Chapter 1. Literature review

As it was said before, one of the promising technologies for energy storage can be the electrocatalytic decomposition of water (electrolysis using a catalyst – a modified electrode surface). This technology is quite expensive because it uses platinum-group metal catalysts.

Electrodes using cubic tungsten carbide can reduce the capital costs of electrocatalysis. A significant improvement in the physical and chemical properties of the material occurs with the use of nanometer-sized powders. To date, there is still no industrial high-performance process for producing such nanopowders.

Plasmodynamic synthesis allows the formation of nanosized particles of cubic tungsten carbide in carbon shells. The need to produce a large amount of ultra- and nanodispersed high-purity tungsten carbide powders makes further research and development of technologies for their production urgent.

1.1. Synthesis of hexagonal tungsten carbide

In the past, the synthesis of tungsten carbide was not subdivided into cubic and hexagonal modifications. However, the synthesis of the cubic modification is more technologically difficult, therefore, historically, the first tungsten carbides were hexagonal.

1.1.1. Direct reaction synthesis

In the past, obtaining of different carbides was based on the direct reaction: tungsten or tungsten oxide powders with carbon was heated for several hours. These processes are significantly expensive because of high synthesis temperatures (1800 ºC) that makes it difficult to obtain nano powders of tungsten carbides, therefore, such a synthesis is not useful for obtaining a material with high properties [2].

1.1.2. Solid-phase reaction method

Solid-phase reaction is relatively simple method in implementation and the possibility of carrying out the reaction without any solvents. Unfortunately, the speed of the solid-phase reaction during thermal activation remains quite low, since it is controlled by the speed of diffusion. The processes of chemical interaction between solid reagents can be significantly accelerated by mechanical activation used in previous method. The most promising in this case is the process of high-temperature mechanochemical synthesis, in which the solid-phase reaction occurs directly during mechanical processing [3].

1.1.3. Direct carburization of tungsten powder

The simplest way to make nanosized WC particles is to use a high-energy mechanical ball mill to reduce the size of the powders to micron or sub-micron sizes. It turned out that high-energy milling is indeed capable of producing nanoscale WC and WC-Co. A variety of grinding methods can be used, including abrasion and planetary mills. Typically, a WC grain size after grinding for more than 100 hours can produce particles down to 10–20 nm [4].

1.1.4. Vapor phase chemical synthesis

Chemical synthesis from the vapor phase is another of the ways to obtain tungsten carbide. Typically, this method involves reducing the tungsten salt precursors with hydrogen and carburizing with a hydrocarbon gas. If tungsten chloride is used as a precursor, and methane and hydrogen gases are used as a reducing substences and carbon source, the reaction equation is as follows:

$$WCl_6(g)+H_2(g)+CH_4(g)=WC(s)+6HCl(g)\ .$$

The free energy of this reaction is from 469 to 630 kJ [4].

1.1.5. Spray conversion method

The spray conversion process was introduced in the beginning of 1990s. It is a three-step process that includes the formation of an aqueous solution, spray drying to form an amorphous powder, and carburization with carbon-containing gases to form phase-pure WC or WC-Co powder. Dissolving tungsten salts, cobalt salts and other additives ensures uniform mixing at the molecular level. This phase uniformity is maintained during the spray drying process, resulting in a course, porous and flowable precursor powder. These features of the particles contribute to the uniform and complete transformation into cermet WC-Co due to the carburization of gases. Grain growth inhibitors can also be included in this process, while facilitating processing options. The process produces micron-sized powder containing nano-sized WC grains dispersed in the binder matrix and allows the inclusion of grain growth inhibitors [4].

The crushed powder is then converted into a nanophase composite powder by gas phase reduction and carburization. It has also been shown that grain growth inhibitors can be included in composite powders to provide uniform dispersion to control grain growth. Another embodiment of the spray conversion process involves coprecipitation of cobalt with tungsten salts such as ammonium paratungstate. The carbide components are mixed at the atomic level, followed by reduction with hydrogen. The average particle size of 20–50 nm is reported for powders prepared in this way [4].

1.1.6. Plasma thermal synthesis

Plasma thermal synthesis is the method with the high processing speed in relation to the synthesis of nanoscale powders, such as high temperature, high quenching rate to form ultrafine powders, and a wide range of reagents. As an example, we can cite a work in which a nanosized composite powder of tungsten carbide (WC_{1-X}) – cobalt containing small amounts of W_2C and W phases was synthesized using ammonium paratungstate and cobalt oxide (Co_3O_4) by thermal plasma.

The resulting composite powders were additionally subjected to additional treatment using hydrogen for the complete carburization of WC_{1-X}, W_2C, and W to the WC phase and for the removal of excess carbon in the synthesized powders [5].

1.2. Synthesis of cubic tungsten carbide

With the discovery of the electrocatalytic properties of the cubic modification of tungsten carbide, interest in its synthesis increases. The synthesis is complicated by the fact that it is not always possible to obtain a pure substance without a hexoganal impurity.

1.2.1. Synthesis by electrical explosion in liquid paraffin

One of the methods is synthesis using electrical explosion of tungsten wire in liquid paraffin. The essence of the experiment was exploding tungsten wires of different diameters by passing high-current electric pulses through them. This was done while the wire was immersed in a liquid-paraffin media. The explosion was studied using a high-speed video camera and by analysis of the voltage and current signals. The different stages of the wire explosion were explained based on an analysis of the recorded signals and simple thermodynamic considerations [6].

In most of the experiments, the wire was sublimated, and the for- mation of carbide particles occurred due to a chemical reaction between the explosion products and the paraffin, as well as the rapid condensation of the vapors. It was found that, regardless of the experimental conditions, the WC_{1-X} phase contained approximately 42.5 % of carbon [6].

1.2.2. Solvent-free synthesis

In the next work a series of tungsten carbide/carbon composites were obtained through a simple solvent-free strategy, where the solid mixture of dicyandiamide and ammonium metatungstate is a precursor. Ultrafine cubic WC_{1-X} nanoparticles (3–4 nm) are generated and uniformly dispersed on carbon nanosheets. This configuration overcomes some disadvantages of conventional carbides/carbon composites and is greatly helpful for electromagnetic dissipation. It is found that the weight ratio of dicyandiamide to ammonium metatungstate can regulate chemical composition of these composites, while less impact on the average size of WC_{1-X} nanoparticles [7].

With the increase in carbon nanosheets, the relative complex permittivity and dielectric loss ability are constantly enhanced through conductive loss and polarization relaxation. The different dielectric properties endow these composites with distinguishable attenuation ability and impedance matching. When dicyandiamide ammonium metatungstate weight ratio is 6.0, the optimized composite can produce good microwave absorption performance, whose strongest reflection loss intensity reaches up to -55.6 dB at 17.5 GHz and qualified absorption bandwidth covers 3.6-18.0 GHz by manipulating the thickness from 1.0 to 5.0 mm. Such a performance is superior to many conventional carbides/carbon composites [7].

1.2.3. Mechanochemical Synthesis

In the last article considered nanocrystalline tungsten carbide powder mixtures of WC, W_2C, and cubic WC_{1-X} was prepared by the mechanochemical method of reactive high energy ball milling WO_3–Mg mixtures containing graphite as a source of carbon for the W phase.

The synthesis is performed in two stages, namely the explosive reactive synthesis of α-W by the reductive reaction of Mg with WO_3 and the diffusion reaction of high activity α-W with C. The chemical regularities of mechanochemical synthesis of the refractory compounds are given. After grinding for 50 hours at a milling rate of 250 RPM, all WO_3 and C diffraction peaks disappeared and only diffraction peaks of tungsten carbides and MgO remained.

The final substance has an average grain size of about 4-20 nm that was obtained after MgO and was removed by HCl solution [8].

1.3. Literature review conclusion

Thus, according to the literature review, in recent years, numerous methods have been proposed for the synthesis of tungsten carbides from various starting reagents. Hexagonal tungsten carbide and its mechanical properties (hardness, refractoriness, wear resistance) have been known to science for a relatively long time and it is widely used in industry for making tools, creating wear-resistant coatings, and jewelry.

Cubic tungsten carbide appeared mainly as a by-product. Separate synthesis cubic tungsten carbide was not interesting until the discovery of its electrocatalytic properties. Also, it should be noted that methods for producing the cubic phase of tungsten carbide are presented only in some works. In addition, almost all methods are multistage technologies that require a large amount of time to obtain nano- and ultrafine powders.

In this work, for the synthesis of the cubic phase of tungsten carbide, the plasmodynamic method was chosen, the distinctive features of which are high speed (operating cycle time less than 1 ms), the possibility of using inexpensive precursors, no need for additional purification of the product, and environmental friendliness. Moreover, plasma-dynamic synthesis makes it possible to obtain a high-purity cubic tungsten carbide powder due to high cooling rates.

Chapter 2. Experimental procedure

2.1. Plasma dynamic synthesis

Plasma-dynamic synthesis is carried out using a coaxial magnetic plasma accelerator (CMPA). It achieves high temperatures and rapid cooling with ultra-fast plasma jets. The starting materials are available and relatively cheap powders of tungsten and carbon black, which are preliminarily placed in an accelerator. When the plasma jet flows into the working chamber, the initial powders are converted into cubic tungsten carbide in the course of the plasma-chemical reaction.

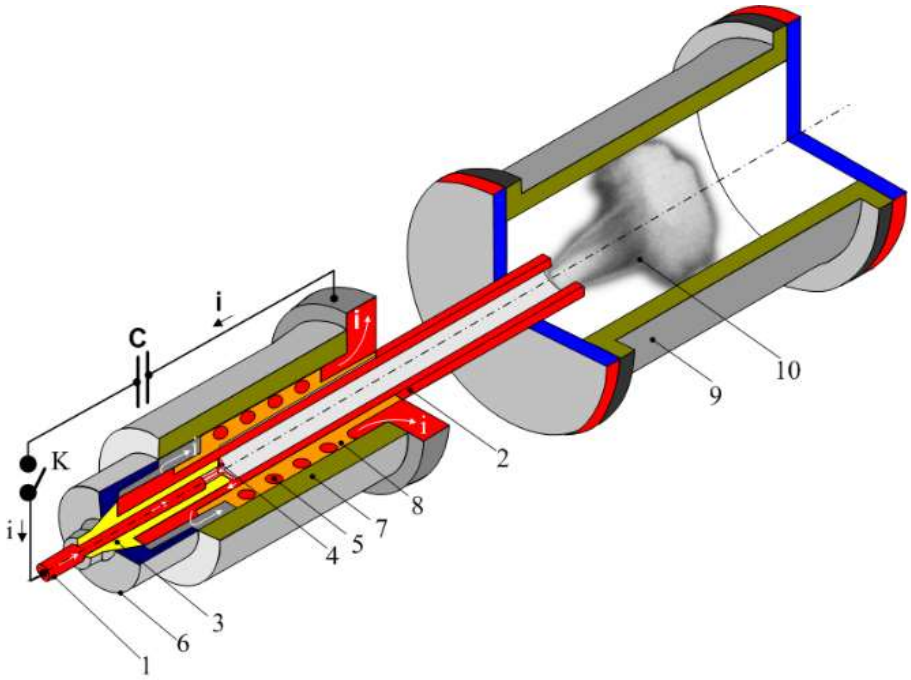

Figure 2.1.1 – Plasmodynamic synthesis system based on the CMPA: 1. Central electrode. 2. Barrel electrode. 3. Insulator of the central electrode. 4. Channel of the formation of the plasma structure. 5. Inductor. 6. Plug. 7. Hull. 8. Insulation. 9. Chamber-reactor. 10. Supersonic jet of electric discharge erosion plasma [9].

The pulsed power supply of the CMPA is carried out from a capacitive energy storage (CES) with a maximum charging capacity C = 28.8 mF at a maximum charging voltage Uchar = 5 kV, which allows accumulating energy up to 360 kJ. The leads of the CMPA electrodes are connected by copper buses to the collector of the power circuit of the CES.

When the key is closed (appendices 1), the ignitron spark gaps are started, the plasma structure formation channel breaks down, the arc plasma discharge ignites, and the discharge current of the capacitor bank begins to flow along the circuit indicated by the arrows to the inductive load. Conversion of electromagnetic energy stored in a capacitive energy storage into kinetic energy of plasma is provided by means of electrodynamic and electrothermal mechanisms. In the process of the passage of the plasma flow through the accelerating channel made of graphite, the material is eroded from its walls, which is involved in the movement of the plasma.

The second precursor (micron tungsten powder or a mixture of tungsten and soot powders) is placed directly in the plasma structure formation channel before the start of the experiment and is transformed into a plasma state under the thermal effect of the flowing discharge current. Thus, at the exit from the accelerating channel, the plasma flow contains both tungsten and carbon required for synthesis. The outflow of a tungsten-carbon plasma jet is produced into a sealed reactor chamber filled with argon under normal conditions. This medium was chosen to exclude the possibility of the formation of other compounds during the course of the plasma-chemical reaction, since argon is a chemically inert gas and does not participate in the formation of the final product.

When the plasma leaves the accelerating channel from the surface of the front of the bow shock wave, the liquid fraction expands, which instantly crystallizes due to the high cooling rate of ~108 K/s. Thus, this makes it possible to ultimately obtain a nanodispersed product that settles on the wall of the reactor chamber and which is collected 1 hour after the experiment.

The measurement of energy parameters (current, voltage) during the experiments was carried out using a voltage divider and a Rogowski transformer, the signals from which are fed to a digital oscilloscope.

2.2. X-ray diffraction analysis

The resulting powdery product was analyzed without preliminary preparation by known methods using modern equipment.

X-ray diffractometry (XRD) was carried out using a Shimadzu XRD7000 X-ray diffractometer (CuKα radiation, λ = 1.54 A) with a Shimadzu CM-3121 graphite monochromator at a step of 0.02 deg and an exposure of 1 s. Qualitative X-ray phase analysis was performed using the PDF2 and structural database. X-ray quantitative phase analysis was performed using the calibration curve method.

For this purpose, X-ray diffraction patterns of specially prepared samples were obtained experimentally: the first type of samples was mixtures of WC and C with various previously known mass ratios, the second type was mixtures of WC and W. Based on the data of X-ray diffraction patterns, the dependences m(WC)/m(C) and m(WC)/m(W) were obtained between the mass ratios of the phases and the ratios of the intensities of the main maxima of the same phases. The calibration curves obtained in this way were used to determine the phase ratio in the synthesis product.

Raman spectroscopy was performed using a T6400-Raman system with an excitation wavelength of λ = 532 nm. All studies were carried out at a laser power of 10 mW and an exposure time of 120 s.

2.3. Electrocatalytic properties analysis

The electrocatalytic properties were investigated by the well-known three-electrode method [10] using a Potentiostat CHI760e electrochemical analyzer (CH Instruments). This method consists in the use of three electrodes, placed in a preselected solution, to which the registration channels from the electrochemical analyzer are connected. The analyzer used included three electrodes: WE (working electrode) – a working electrode on which the material under study was applied; RE (reference electrode) – a reference electrode consisting of Ag/AgCl; CE (counter electrode) – a counter electrode, which was a platinum filament (figure 2.3.1). After that, the required mode was selected in the analyzer software environment, in which the operating parameters were set. Then a voltage was applied to the electrodes, and the device recorded the current flowing in the liquid medium. The value of this current was used to determine the catalytic activity of the samples.

To carry out electrocatalytic studies on hydrogen production, it was initially necessary to prepare a working electrode by applying the obtained platinum-modified tungsten carbide powder to its surface. For this, the working glassy carbon electrode was polished with Al_2O_3 paste (500 nm) and washed in deionized water. The mixture of the prepared catalyst (20 mg) was dispersed in 5 ml of ethanol. The resulting ink

containing the catalyst was applied with a pipette onto a glassy carbon electrode 3 mm in diameter. After air drying, 5 ml of 5% Nafion was additionally applied to the electrode surface to protect the catalyst from damage in the working solution. Then the working electrode was dried in air. All three electrodes were placed in an H_2SO_4 solution (0.5 M).

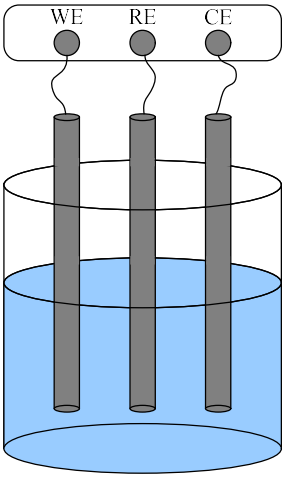

Figure 2.3.1 – Electrochemical analyzer scheme. WE – working electrode; RE – reference electrode; CE – counter electrode

The electrochemical analyzer used is presented in figure 2.3.2.

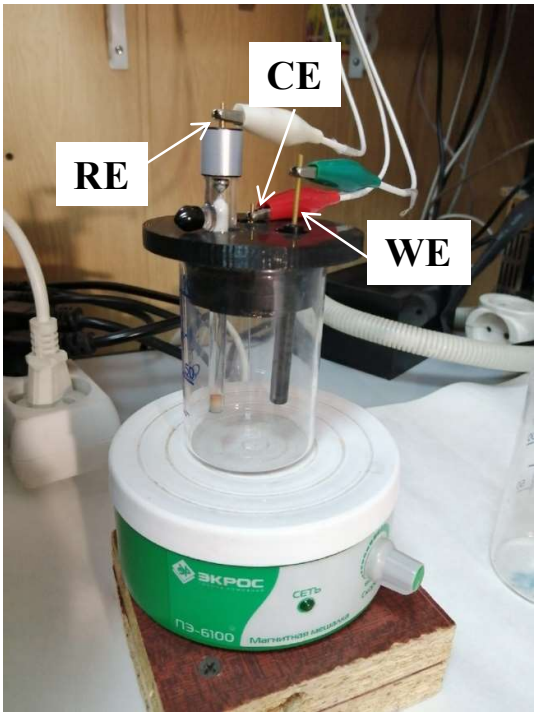

Figure 2.3.2 – Electrochemical analyzer

The shooting range selected in the potentiometer software was calculated according to the equation:

$$E_{Ag/AgCl} = E_{RHE} - 0{,}059 \cdot pH - 0{,}1976\,,$$

where $E_{Ag/AgCl}$ – working range of shooting with this type of reference electrode;

E_{RHE} – working range of shooting in the ideal case of using a reference hydrogen electrode;

pH – solution pH.

Using this equation, the range of application was determined for the synthesis of hydrogen, and for the reaction of hydrogen oxidation. Thus, the operating range of regulation in the hydrogen reaction is (0.0-1.4) V.

To study the electrocatalytic activity of cubic tungsten carbide in the hydrogen oxidation reaction, a working electrode was prepared in a similar way, on which a solution was applied, consisting of 10 mg of the synthesized powder and 5 ml of deionized water. The top of this solution was also coated with ml of 5% Nafion solution. These studies were carried out in a CH_3OH methanol solution (0.5 M).

2.4. Other procedures

The oxidation process was studied using differential thermal and thermogravimetric analyzes (DTA-TG) on an SDTQ600 thermal analyzer by heating in air in the temperature range from 50 °C to 1000 °C at a rate of 10 °C/min. The resulting powders were annealed in air in an oven at a heating rate of 10 °C/min and natural cooling.

Heat treatment in vacuum was carried out at a heating rate of 100 °C/min using the Advanced Technologies SPS-10 spark plasma sintering system. The holding time was 15 minutes. The cooling rate was determined by the parameters of the water-cooling circuit and was about 50 °C/min.

Transmission electron microscopy (TEM) was performed using a JEOL JEM 2200 F microscope with an accelerating voltage of up to 200 kV. To decipher the electron microdiffraction pattern in the selected areas, a gold standard sample was used.

Scanning electron microscopy (SEM) was performed on a Jeol JSM 7500F scanning microscope.

The measurement of nanohardness was carried out using the NANO Hardness Tester NHT-S-AX-000X. The load on the indenter was 30 mN.

2.5. Experiment results

A series of experiments was carried out to obtain a dispersed powder based on cubic tungsten carbide with different content of free carbon by changing the ratio of the initial precursors C/W in different ranges presented in table 2.5.1.

Table 2.5.1 – Initial data of experiments on obtaining powder of cubic tungsten carbide

Experiment	ν(C)/ν(W)	m(C), g	m(W), g
1	64.93	0.382	0.091
2	5.62	0.150	0.411
3	2.14	0.070	0.507
4	1.7	0.056	0.508
5	1.37	0.020	0.252
6	0.63	0.020	0.507

The resulting diffractograms are shown in the figure 2.5.1.

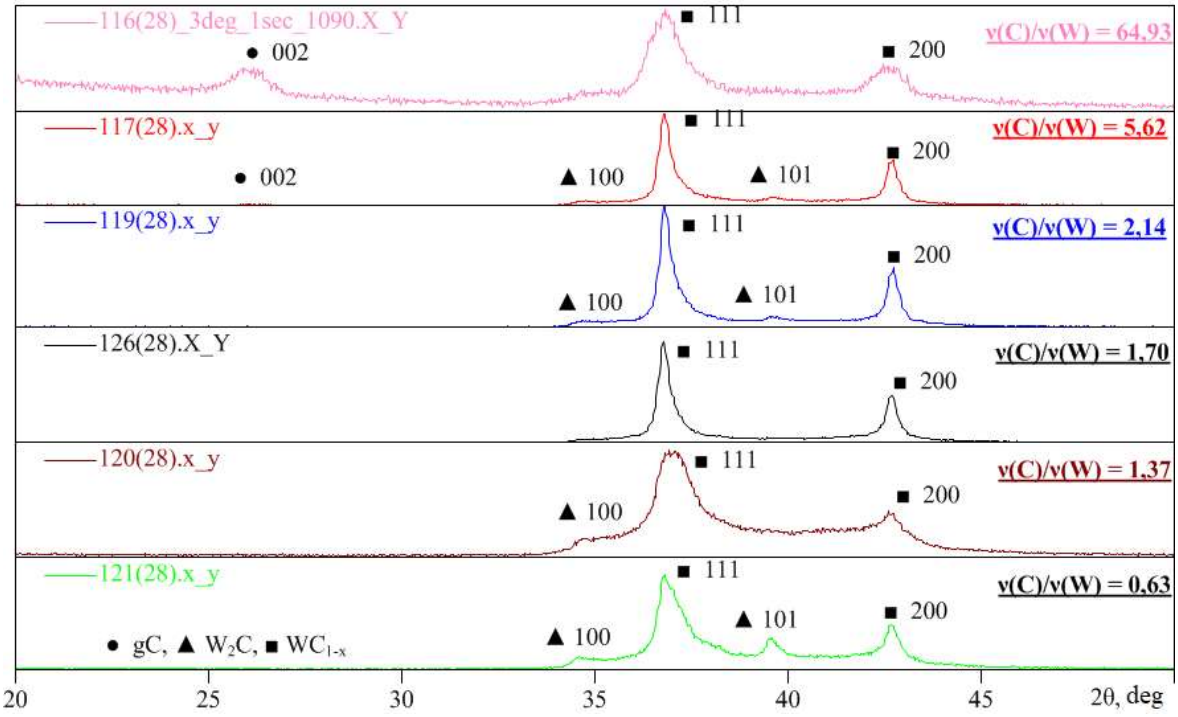

Figure 2.5.1 – X-ray phase analysis for different C/W ratios

Graph 2.5.2 was built based on the data in Figure 2.5.1 and interpolation. As we can see, the most effective ratio of 1.7 gives the highest proportion of tungsten carbide.

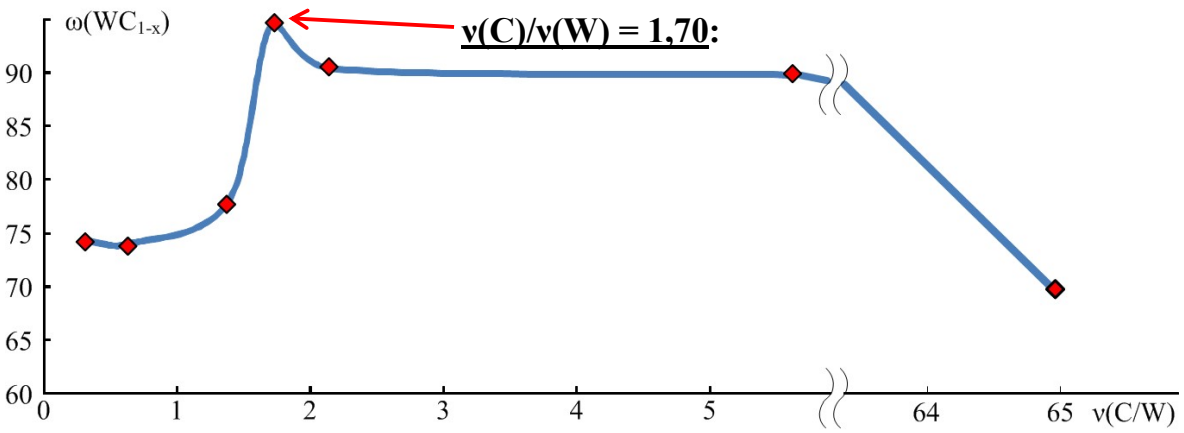

Figure 2.5.2 – Dependence of WC_{1-x} concentration on the C/W ratio

In order to estimate the particle size, transmission electron microscopy was performed. The results are shown in the figure 2.5.3.

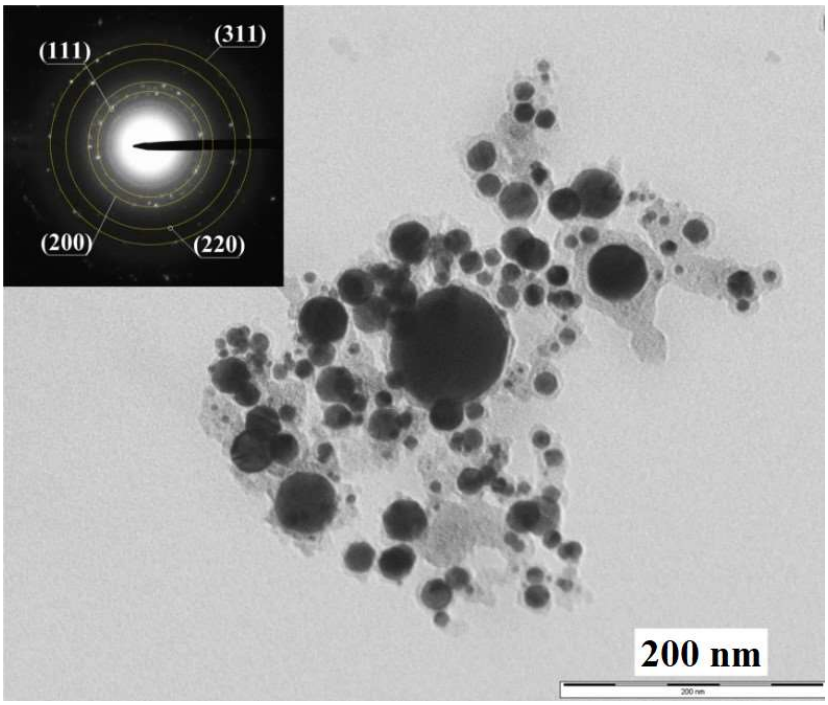

Figure 2.5.3 –Electron microscopy results

The dominant part of WC_{1-X} particles has a size less than 50 nm. In addition, the distribution maximum falls on the range from 10 to 30 nm.

Processing of measurement results

- LSV curves are plotted for each sample. For this, the obtained current values are recalculated to a unit area (current density to cm^2), with an electrode diameter of 3 mm^2;
- One best slope LSV / overvoltage curve is selected for each product;
- This LSV curve is used to construct Tafel curves – dependences U = f (logI(mA/cm^2));

- Tafel slope values are calculated;
- The η_1 values are calculated (overvoltage at 1 mA/cm^2);
- η_{10} (overvoltage at 10 mA/cm^2);
- η_{10}-η_1 (overvoltage difference).

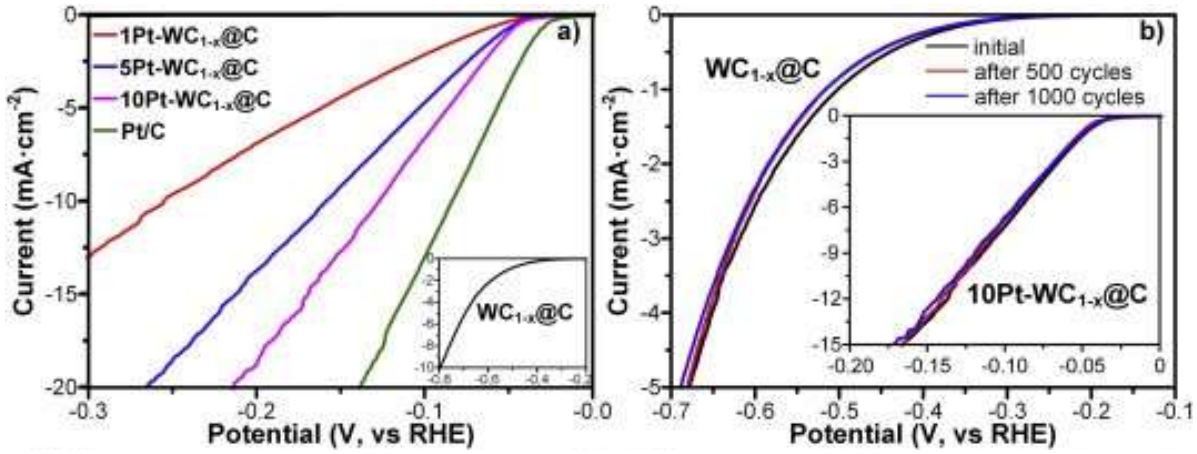

Figure 2.5.4 – Hydrogen evolution performance of different WC_{1-x}@C-based catalysts in comparison with commercial Pt/C sample: a) LSV polarization curves in N_2 saturated 0.5 M H_2SO_4 at a scan rate 1 mV s^{-1}; b) Polarization curves recorded before and after 500 and 1000 CV cycles at a scan rate of 5 mV s^{-1} [11].

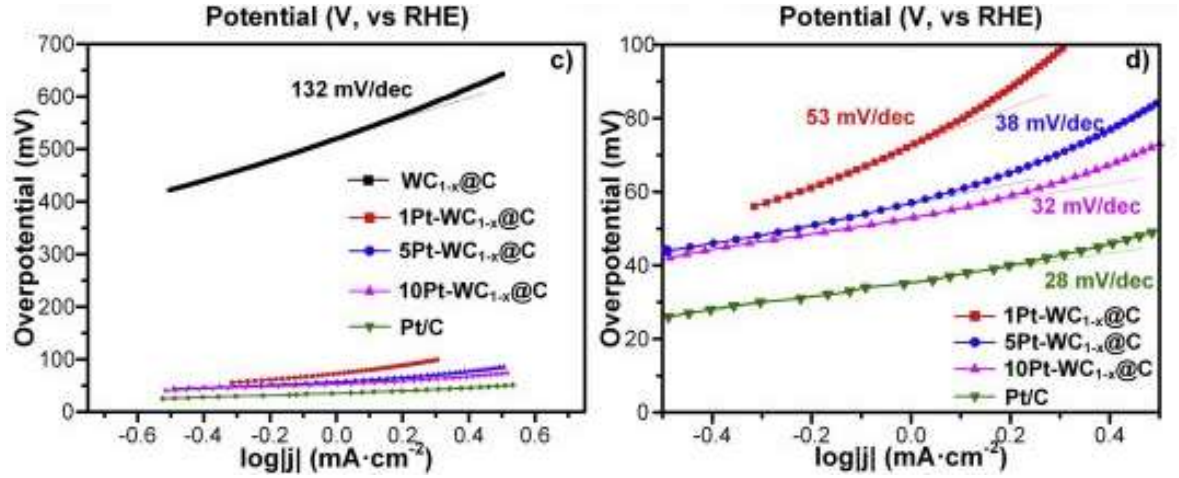

Figure 2.5.5 – Hydrogen evolution performance of different WC_{1-x}@C-based catalysts in comparison with commercial Pt/C sample: c) Hydrogen evolution reaction (HER) Tafel plots (log j versus potential for linear voltammetry);

d) enlarged Tafel plots for Pt-modified samples [11].

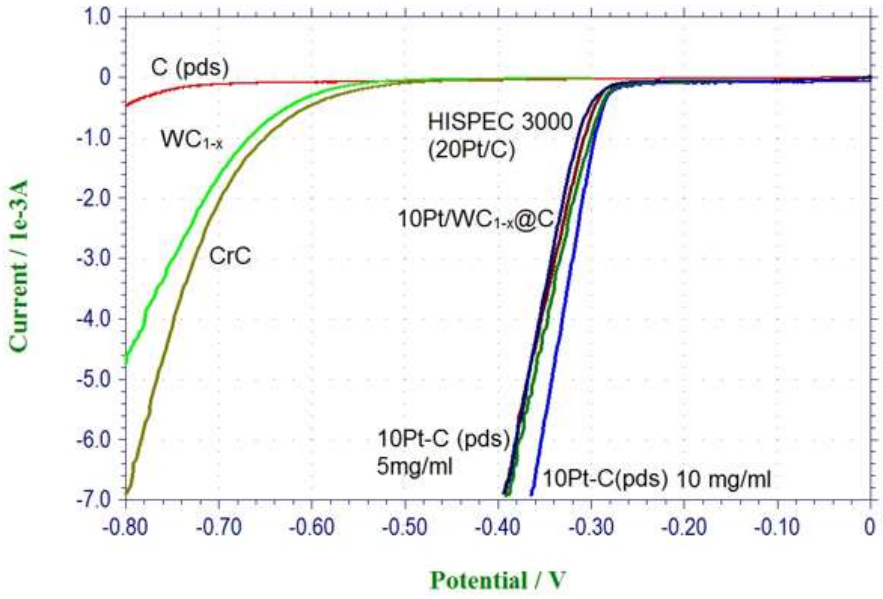

Figure 2.5.6 – LSV polarization curves in the different scale [11].

2.6. Experiment conclusion

A sample modified with 10% platinum has the closest value of the slope of the curve. And as the amount of platinum decreases, this ratio increases. Nevertheless, the data obtained show that cubic tungsten carbide can be used as a substitute for platinum in the hydrogen production reaction. This can have a positive effect on the cost of the produced hydrogen, since the percentage of platinum in the catalysts can be reduced and the reactants used to prepare catalysts based on cubic tungsten carbide are less expensive than commercial catalysts.

An important factor by which the prospects of using a catalyst are judged is its stability (the number of cycles that a catalyst can work out without practically losing its activity, Figure 2.5.4 b). The results of studying the stability of the prepared catalyst containing 10% platinum show that the sample has good stability, since after 1000 potential operating cycles, its activity practically did not change. The rest of the catalysts showed similar stability during research.

WC_{1-X} is not a very good electrolyte by itself. However, it can be used as a cocatalyst, significantly increasing the efficiency of electrocatalysis with a low Pt content.

In the future, it is planned to conduct a series of experiments on the plasma dynamic synthesis of dispersed materials with a high content of WC_{1-X}, with different content of free carbon (WC_{1-X} / C), with different content of crystalline phases (WC_{1-X} / W_2C / WC) in the composition of the synthesis product. Direct measurements of the electrocatalytic activity of these materials will be carried out using the three-electrode cell method and various electrolytes, as well as materials with various amounts of Pt additives (1, 5, 10%).

Chapter 3. Energy accumulation ways review

Energy accumulation may be compared by different ways. For instance, there are 2 parameters used in order to describe the effectiveness of energy storage: specific energy and specific power. E.g., battery can give us relatively big amount of energy, however, capacitor can provide a thousand times more power. In order to consider both of these values Ragone plot was invented [12]. Usually, one energy accumulation may provide us either specific energy or specific power, that is why we need both capacitors and batteries.

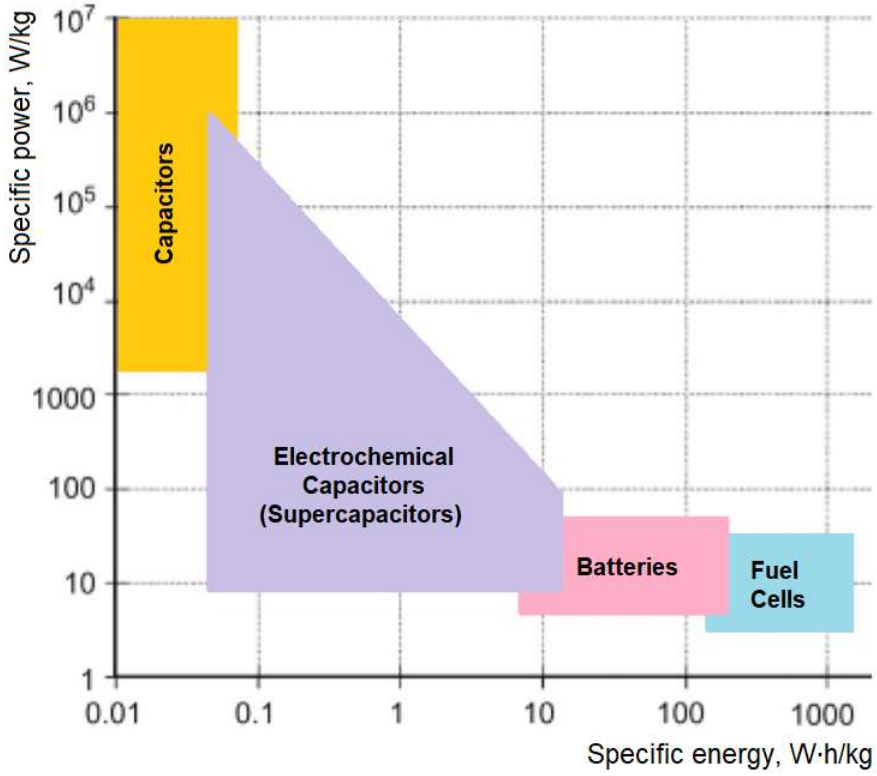

Figure 3.1 – Energy Storage Ragone plot [13]

3.1. Hydrogen energy storage

In hydrogen energy storage, hydrogen may be produced either directly (e.g., photoconversion) or through electrolytic methods, stored for a period of time, and then oxidized or otherwise chemically reacted to recover the input energy (figure 3.1.1).

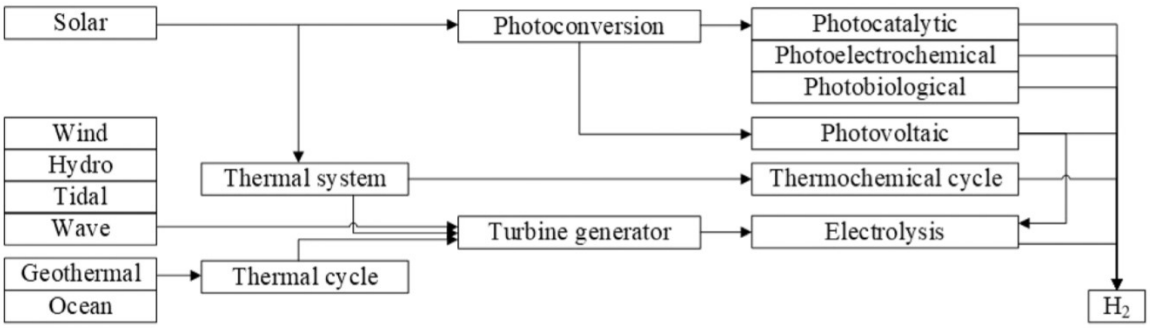

Figure 3.1.1 – Production of hydrogen using renewable energy sources [13]

One common method of hydrogen production is by splitting water. The energy required for this process can be provided from fossil fuels and renewable or other energy sources. Energy from renewable sources is often intermittent and needs to be stored before it is needed.

The storage of hydrogen is a substantial challenge, especially for automotive applications. Hydrogen has a low energy density on a volume basis compared to the other fuels, requiring a much larger fuel tank for a vehicle operating on hydrogen rather than petrol/diesel. Furthermore, hydrogen is the lightest of all elements and harder to liquefy than methane and propane. Due to its low density and also its small molecular size, it can leak from containment vessels. Hydrogen can be stored in its pure form as a compressed gas or as a cryogenic liquid or in a mixed-phase (hydrogen slush). Liquefaction of hydrogen and pressurization of a cryogenic liquid in order to achieve higher density in a liquid or mixed-phase state both require a large amount of energy and specialized infrastructure. In adsorptive storage, hydrogen is absorbed to and released from porous networks such as zeolites, metal−organic frameworks, clathrate hydrates, various carbon materials (e.g., nanotubes, fullerenes and graphene), and conventional organic polymers. This process can occur for several cycles without decomposition of the solid or loss of gas. In chemical storage, hydrogen is stored in chemical bonds with other elements in a hydrogen-rich material, in solid or liquid phases. Solid-phase systems include metal and non-metal hydrides, amines, amides, and ammonia-like complexes. Liquid carriers include N-ethylperhydrocarbazole, alcohols and formic acid [13].

Fuel cells are low power-density devices like batteries that convert chemical energy to electricity. They exhibit energy efficiencies of approximately 70–80%, while some power plants (e.g., combined cycle units) can achieve efficiencies as high as 60%. Fuel cells use oxygen and a fuel such as hydrogen. They can be combined with supercapacitors to improve their power densities [13].

3.2. Electrochemical and battery energy storage

Electrical energy can be stored electrochemically in batteries and capacitors. Batteries are mature energy storage devices with high energy densities and high voltages. Various types exist including lithiumion (Li-ion), sodium-sulfur (NaS), nickel-cadmium (NiCd), lead acid (Pb-acid), lead-carbon batteries, as well as zebra batteries (Na-$NiCl_2$) and flow batteries. Capacitors store and deliver energy electrochemically, and can be classified as electrostatic capacitors, electrolytic capacitors, and electrochemical capacitors. Among these three types, electrochemical capacitors, also called

supercapacitors or ultracapacitors (UCs), have the greatest capacitance per unit volume due to having a porous electrode structure [13].

Among the various battery types, lithium batteries are playing an increasingly important role in electrical energy storage because of their high specific energy (energy per unit weight) and energy density (energy per unit volume) [13].

However, due to the widespread availability and low price of sodium, and the similarity of Li and Na insertion chemistries, Na-ion batteries could become the future low-cost batteries for smart electric grids that integrate renewable energy sources [13].

Electrochemical capacitors have high storage efficiencies (>95%) and can be cycled hundreds of thousands of times without loss of energy storage capacity. Energy efficiency for energy storage systems is defined as the ratio between energy delivery and input [13].

3.3. Other energy accumulation ways

The following energy storage technologies can also be distinguished [13]:

- Flywheel energy storage;
- Magnetic energy storage;
- Compressed air energy storage;
- Pumped hydro energy storage.

Some technologies are mature enough and their research is not so promising. Some have only narrow application, for some there is not enough research, so less attention is paid to them.

3.4. Energy accumulation ways conclusion

Batteries are likely to be the cheapest energy storage with relatively fewer cycle applications. It is expected that performance and cost will be limiting factors as they apply to many storage applications.

In pumped hydro energy storage systems, advances in turbine design are needed to improve performance. Among compressed air energy storage systems, isothermal compressed air energy storage is still an emerging technology, but is ultimately likely to provide a better efficiency than the compressed air technology due to its more efficient compression operation

Nowadays hydrogen energy storage systems are not very effective in componence with batteries. However, authors [13] report: “Among the various energy storage system categories, hydrogen energy storage systems appear to be the one that can result in large changes to the current energy system. Several technological, economic, social and political barriers need to be overcome before hydrogen technologies can be used in large scale applications”. That is why investigation in this area are relevant.

Chapter 4. Optimal solution selection

All electrolyzers use two electrodes, oxygen is produced on one and hydrogen on the other. Some kind of membrane is required to separate the oxygen and hydrogen gases. These membranes create a high resistance to flow and therefore increase the time and cost of producing hydrogen.

Membraneless electrolysis paves the way for cost reduction. Removing the membrane and associated ancillary components not only reduces capital costs, but also increases operational flexibility. Membranes have a limited operating temperature. Exceeding this setpoint affects the life of the electrolytic cell and the purity of the gas it produces. Membraneless operation eliminates these limitations, allowing operation in more efficient conditions such as high engine temperatures.

Membraneless electrolyzers consist of less components that leads to more effective cheapening of electrodes. Typically, noble metal electrodes such as platinum are used, making electrodes an expensive part of the electrolyzer. We will consider membraneless electrolyzers application of tungsten carbide catalyst. All calculations will be made in specific and relative units.

4.1 Capex and opex estimation

4.1.1. Normal membraneless electrolyzer

In order to estimate capital expenditures (capex) of membraneless electrolyzer systems, we can use data of commercial electrolyzers: polymer electrolyte membrane (PEM) electrolyzer systems. Such systems have wide application and enough of data. According to the [1], for a constant electrolyzer lifetime of 10 years, capex based on the capital costs of today's commercial PEM electrolyzer systems are around 1,000–1,500 $ / kW.

Article [1] also provides us structure of the PEM capex that is presented in table 4.1.1.1.

Table 4.1.1.1 Capex for a PEM Electrolysis System [1]

Component	System Cost, %
Bipolar plates	30.6
Current collectors	10.2
MEA manufacturing	6.0
Membranes	3.0
Anode catalyst	3.6
Cathode catalyst	1.2
Other stacks	5.4
Power electronics	15.0
Gas conditioning	10.0
Balance of plant	15.0

However, as it said before, PEM systems use a plenty of additional expensive components which makes cheapening of electrolyzer impractical. If we exclude the components of PEM system and leave

components of membraneless electrolysis system (anode catalyst, cathode catalyst), we can estimate the capital costs structure. We also assume that our power plant is renewable that is why it already has equipment for plant balance. The results are presented in table 4.1.1.2.

Table 4.1.1.2 – Capex for a Membraneless Electrolysis System (based on data from [1])

Component	System Cost (%)
Anode catalyst	3.6
Cathode catalyst	1.2
Power electronics	15.0
Gas conditioning	10.0

Taking into account the operating efficiency of the membraneless electrolyzer equals to 61% [14], we recalculate specific capex for the membraneless electrolyzer with platinum electrodes:

$$Capex_{Pt} = 1250 \cdot (0.036 + 0.012 + 0.15 + 0.1) = 1250 \cdot 0.298 = 372.5 \, \$ \, / kW$$

The operating cost of hydrogen production is mainly determined by the cost of the electricity used in it. Electricity price for hydrogen produced by membraneless technology is taken as 0.07 $/kWh [15]. We can find value of specific opex for membraneless electrolyzer.

$$Opex_{Pt} = \frac{0.07 \, \$ \, / kWh}{0.61} = 0.1148 \, \$ \, / kWh$$

4.1.2. Modified membraneless electrolyzer

In order to find the capex of the modified electrode, (in equal hydrogen values), we need to take into account:

- cost of materials used;
- cost of production.

In production of electrodes we need tungsten, platinum, and carbon. In comparison with tungsten and platinum, carbon is negligible, we will not take it into account in the calculations.

Assuming that platinum costs 30166 €/kg [16], tungsten 75 $/kg [17] and euro exchange rate 1.15 on 06.02.2022 [18], we can find the ratio of capital costs for anode and cathode:

$$k_{pt/tu} = \frac{C_{pt}}{C_{tu}} k_{\$/€} = \frac{30166 \, € \, / \, kg}{75 \, \$ \, / \, kg} 1.15 \, \$ \, / \, € = 462.55$$

And assuming that the new electrode consists of 10% platinum and 90% tungsten we can obtain material costs ratio. The same calculations used for 5% and 1% of platinum:

\

$$\backslash k_{pt/5\%pt} = \frac{C_{pt}}{0.05 \cdot C_{pt} + 0.95 \cdot C_{tu}} = \frac{k_{pt/tu}}{0.05 \cdot k_{pt/tu+pt} + 0.95} = \frac{462.55}{0.05 \cdot 462.55 + 0.95} = 19.2$$

$$k_{pt/1\%pt} = \frac{C_{pt}}{0.01 \cdot C_{pt} + 0.99 \cdot C_{tu}} = \frac{k_{pt/tu}}{0.01 \cdot k_{pt/tu+pt} + 0.99} = \frac{462.55}{0.01 \cdot 462.55 + 0.99} = 82.1$$

We know that materials for electrode costs $k_{pt/x\%pt}$ times cheaper, however, production cost is still unknown. Another thing to consider is that industrial size platinum electrodes are quite simple in design – they are actually sheets of material, they can be produced in a steel mill and cost about the same as the material.

Assuming that electrode production takes 25% money of origianl electrode (0.9% of capex for anode and 0.3% for cathode), we can recalculate fractions of components relative to the PEM electrolyzer capex (1250 $/kW).

Table 4.1.2.1 – Capex ratio of modified electrolyzer relative to the membraneless electrolysis system (based on data from [1])

Component	System Cost, %			
	Membraneless	For 1% Pt	For 5% Pt	For 10% Pt
Anode catalyst	3.6	0.93	1.04	1.18
Cathode catalyst	1.2	0.31	0.35	0.39

Then, final capex:

$$Capex_{1\%Pt} = 1250 \cdot (0.0093 + 0.0031 + 0.15 + 0.1) = 328\ \$/kW$$

$$Capex_{5\%Pt} = 1250 \cdot (0.0104 + 0.0035 + 0.15 + 0.1) = 329.88\ \$/kW$$

$$Capex_{10\%Pt} = 1250 \cdot (0.0118 + 0.0039 + 0.15 + 0.1) = 332.12\ \$/kW$$

The difference between modified and normal electrolyzer in efficiency, i.e. electricity consumption. It was found that new catalysts operate worse than platinum one (efficiency is lower). It varies depending on amount of platinum in electrode (from 0 to 10%). We can find new operating efficiency using Tafel plots presented before (figure 4.1.2.3).

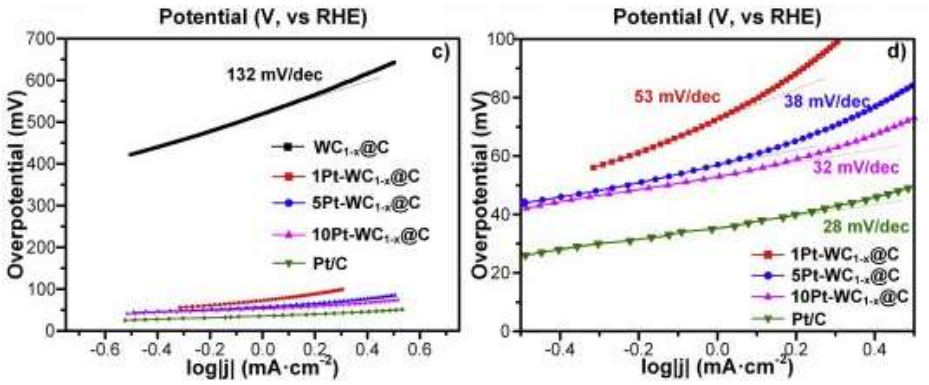

Figure 4.1.2.3 – HER Tafel plots in different scales [11].

These plots show rate of an electrochemical reaction to the overpotential, in other words, how much of voltage should we apply in order catalyst reaction for some amount. Relative difference between these rates can estimate us relative efficiency.

$$n_{Pt} / \eta_{0\%Pt} = \frac{28\ mV / dec}{132\ mV / dec} = 0.212;$$

$$n_{Pt} / \eta_{1\%Pt} = \frac{28\ mV / dec}{53\ mV / dec} = 0.528;$$

$$n_{Pt} / \eta_{5\%Pt} = \frac{28\ mV / dec}{38\ mV / dec} = 0.737;$$

$$n_{Pt} / \eta_{10\%Pt} = \frac{28\ mV / dec}{32\ mV / dec} = 0.875.$$

We can interpolate this data to figure 4.1.2.4:

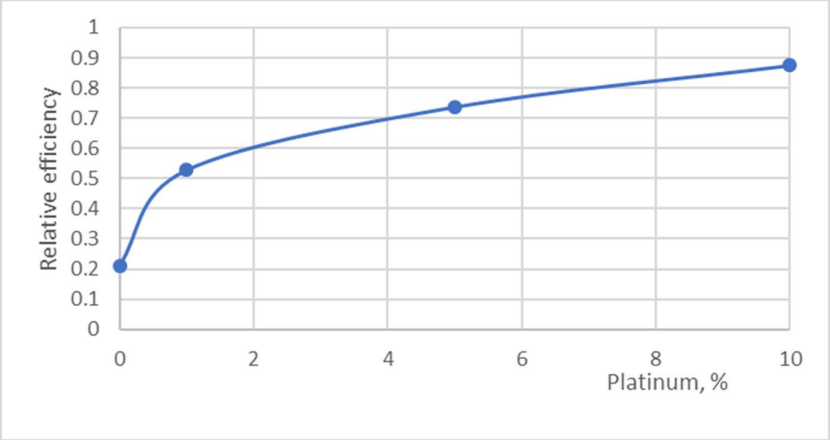

Figure 4.1.2.4 – Dependence of relative efficiency on the amount of platinum

It can be seen that efficiency changes quite linearly since 1 % of platinum.

Using this data, we can estimate opex for modified electrolyzers:

$$Opex_{1\%Pt} = \frac{0.1148\ \$ / kWh}{0.528} = 0.2173\ \$ / kWh;$$

$$Opex_{5\%Pt} = \frac{0.1148\ \$ / kWh}{0.737} = 0.1557\ \$ / kWh;$$

$$Opex_{10\%Pt} = \frac{0.1148\ \$ / kWh}{0.875} = 0.1311\ \$ / kWh.$$

4.1.3. Steam Methane Reforming

Capex considerably varies depending on installed power of the steam methane reforming facility. Authors [19] estimate steam methane reforming capex between 350 €/kW and 530 €/kW for large scale hydrogen production (50 000 – 100 000 Nm^3 /h which is 4494 – 8988 kg/h). We can take the average value of it and convert it to $/kW for 1.15 $/€ [18]:

$$Capex_{SMR} = \frac{530 € / kW + 350 € / kW}{2} 1.15 \$ / € = 506 \$ / kW$$

Mainly, steam methane reforming opex consists of the cost of feedstock, power and CO_2 emission allowances as well as other operation and maintenance costs. Total opex for hydrogen produced by steam methane reforming was estimated as 44.1 €/MWh [19] with following prices.

Table 4.1.3 – The opex structure of steam reforming based on data from [19]

Input costs	Value
Methane	88.21 %
Electricity	1.52 %
CO_2 emission	8.71 %
Other maintenance	1.56 %

Values from table 4.1.3 were calculated using following prices for 2018:

Table 4.1.3 – Operational costs values [19]

Input costs	Value
Natural gas, €/MW	20
Electricity, €/MW	30
Carbon tax, €/t_{CO2}	10

Electricity price for this reforming was 30 €/MW, lifetime of facility is 10 years [19]. Considering new electricity price (0.07 $/kWh [15]) and euro exchange rate 1.15 [18], we can estimate opex in $/kW:

$$Opex_{\text{reforming}} = \left(Opex_{tot} - Opex_{el} + Opex_{el} \cdot \frac{P_{el\ new}}{r_{exch} \cdot P_{el\ new}} \right) \cdot r_{exch} \ ;$$

$$Opex_{\text{ref}} = \left(100\% - 1.52\% + 1.52\% \cdot \frac{0.07 \$ / kWh}{1.15 \$ / € \cdot 0.03 € / kWh} \right) \cdot 0.0441 € / kWh \cdot 1.15 \$ / € = 0.0515 \$ / kWh$$

Where: $Opex_{tot}$ – share of total initial opex, %; $Opex_{el}$ – share of initial opex value for electricity, k€/a; $P_{el\ new}$ – new electricity price used for electrolyzers calculations, 0.07 $/kWh; r_{exch} – exchange rate, $/€.

4.2 Comparison of the selected variants

We can summarize all the processed information in the table 4.2.1.

Table 4.2.1 – Opex and specific capex summary

Selected variants	Specific capex, $/kW	Opex, $/kWh
Steam methane reforming	506	0.0515
Membraneless electrolyzer	372.5	0.1148
Modified electrolyzer (1% Pt)	328	0.2173
Modified electrolyzer (5% Pt)	329.88	0.1557
Modified electrolyzer (10% Pt)	332.12	0.1311

Hydrogen contains 33.33 kWh/kg of energy [20]. Sales price of hydrogen for energy application in Europe estimated as 4-6 €/kg [21]. Then, the sales price in $/kWh is;

$$P_{H_2} = \frac{5 \cdot 1.15}{33.33} = 0.173\ \$/kWh$$

We will make follow assumptions:

- Our electrolyzers and steam methane reformer will operate 1/3 of time: 8766/3=2922 hours annually;
- We invest in 1 kW of each equipment (although it is impossible for steam methane reforming in the such scale);
- Annual inflation rate is not considered assuming that hydrogen price increase will compensate opex increase;
- Revenue from all projects is equal to each other;
- Corporate tax is average corporate tax in Europe – 21.7% [22];
- Discount rate 4.84%.

The overall data for economical models is shown in table 4.2.2.

Table 4.2.3 – Economic model parameters

Tax, %	rd, %	Lifetime, years	Work time, h/year	H_2 price, $
21.7	4.84	10	2922	0.173

Tables 4.2.3-4.2.7 present economic models for different types of energy storage.

Table 4.2.3 – Economic model for steam methane reforming

	0	1	2	3	4	5	6	7	8	9	10
Capex	-506										
Depr.		-51	-51	-51	-51	-51	-51	-51	-51	-51	-51
Opex		-151	-151	-151	-151	-151	-151	-151	-151	-151	-151
Rev.		506	506	506	506	506	506	506	506	506	506
EBT	0	304	304	304	304	304	304	304	304	304	304
EAT	0	238	238	238	238	238	238	238	238	238	238
CF	-506	289	289	289	289	289	289	289	289	289	289
DCF	-506	276	263	251	239	228	218	208	198	189	180
CDCF	-506	-230	32	283	522	751	968	1176	1374	1562	1743

Table 4.2.4 – Economic model for membraneless electrolyzer

	0	1	2	3	4	5	6	7	8	9	10
Capex	-373										
Depr.		-37	-37	-37	-37	-37	-37	-37	-37	-37	-37
Opex		-335	-335	-335	-335	-335	-335	-335	-335	-335	-335
Rev.		506	506	506	506	506	506	506	506	506	506
EBT	0	133	133	133	133	133	133	133	133	133	133
EAT	0	104	104	104	104	104	104	104	104	104	104
CF	-373	141	141	141	141	141	141	141	141	141	141
DCF	-373	135	129	123	117	112	106	102	97	92	88
CDCF	-373	-238	-109	14	131	242	349	450	547	639	727

Table 4.2.5 – Economic model for modified electrolyzer (1% Pt)

	0	1	2	3	4	5	6	7	8	9	10
Capex	-328										
Depr.		-33	-33	-33	-33	-33	-33	-33	-33	-33	-33
Opex		-635	-635	-635	-635	-635	-635	-635	-635	-635	-635
Rev.		506	506	506	506	506	506	506	506	506	506
EBT	0	-162	-162	-162	-162	-162	-162	-162	-162	-162	-162
EAT	0	-127	-127	-127	-127	-127	-127	-127	-127	-127	-127
CF	-328	-94	-94	-94	-94	-94	-94	-94	-94	-94	-94
DCF	-328	-90	-86	-82	-78	-74	-71	-68	-65	-62	-59
CDCF	-328	-418	-504	-586	-664	-738	-809	-877	-942	-1003	-1062

Table 4.2.6 – Economic model for modified electrolyzer (5% Pt)

	0	1	2	3	4	5	6	7	8	9	10
Capex	-330										
Depr.		-33	-33	-33	-33	-33	-33	-33	-33	-33	-33
Opex		-455	-455	-455	-455	-455	-455	-455	-455	-455	-455
Rev.		506	506	506	506	506	506	506	506	506	506
EBT	0	18	18	18	18	18	18	18	18	18	18
EAT	0	14	14	14	14	14	14	14	14	14	14
CF	-330	47	47	47	47	47	47	47	47	47	47
DCF	-330	45	43	41	39	37	35	34	32	31	29
CDCF	-330	-285	-243	-202	-164	-127	-91	-58	-26	5	34

Table 4.2.7 – Economic model for modified electrolyzer (10% Pt)

	0	1	2	3	4	5	6	7	8	9	10
Capex	-332										
Depr.		-33	-33	-33	-33	-33	-33	-33	-33	-33	-33
Opex		-383	-383	-383	-383	-383	-383	-383	-383	-383	-383
Rev.		506	506	506	506	506	506	506	506	506	506
EBT	0	89	89	89	89	89	89	89	89	89	89
EAT	0	70	70	70	70	70	70	70	70	70	70
CF	-332	103	103	103	103	103	103	103	103	103	103
DCF	-332	98	94	89	85	81	78	74	71	67	64
CDCF	-332	-234	-140	-51	34	116	193	267	338	405	469

Discounted cashflows were summed up and NPV values of projects were calculated as well as equal annual annuity. Table 4.2.8 presents the results.

Table 4.2.8 – Selected variants comparison

	Steam methane reforming	Membraneless electrolyzer	Modified electrolyzer		
			1% Pt	5% Pt	10% Pt
NPV, $	1742.59	727.46	-1062.03	33.77	469.14
EAA, $	223.92	93.48	-136.47	4.34	60.28

Chapter 5. Sensitivity analysis of electrolysis devices implementation

5.1 Tornado diagrams

In order to estimate importance of input parameters, sensitivity analysis was performed. Every input parameter was change by ± 10% (efficiency was change in absolute value, other values were changed in relative values).

Figures 5.1-5.5 demonstrate tornado diagrams for 5 variants of projects for 5 input parameters; capex, tax value, discount rate, working hours and efficiency.

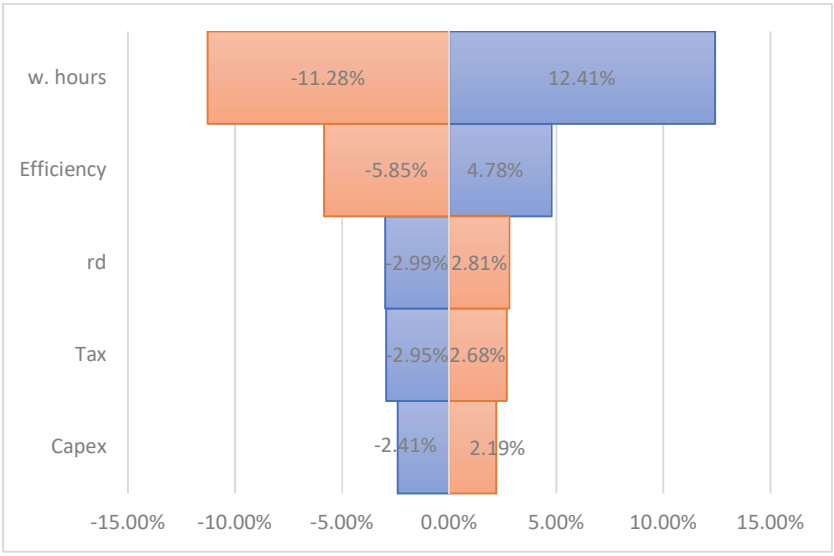

Figure 5.1 – Tornado diagram for NPV of steam methane reforming

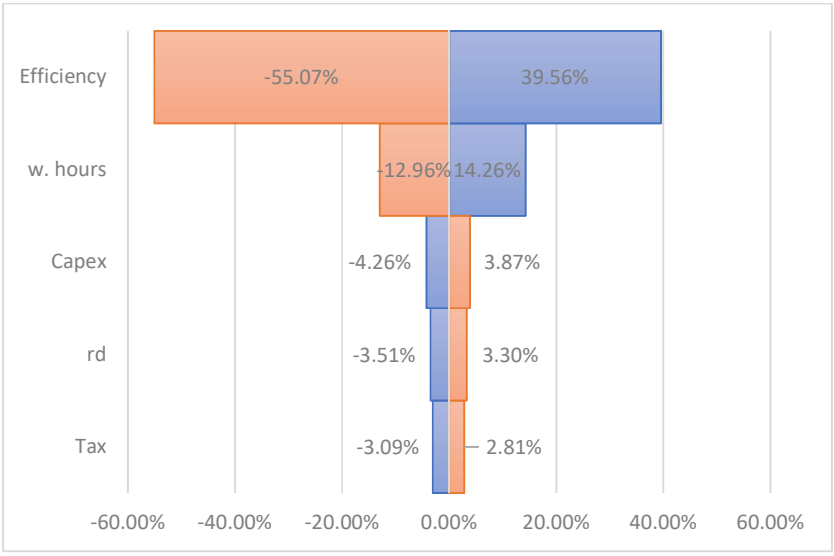

Figure 5.2 – Tornado diagram for NPV of membraneless electrolyzer

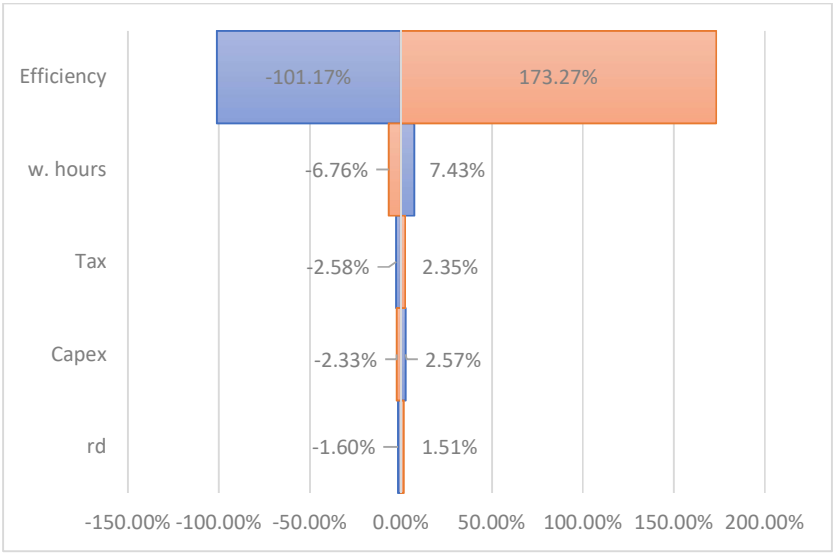

Figure 5.3 – Tornado diagram for NPV of modified electrolyzer (1% of Pt)

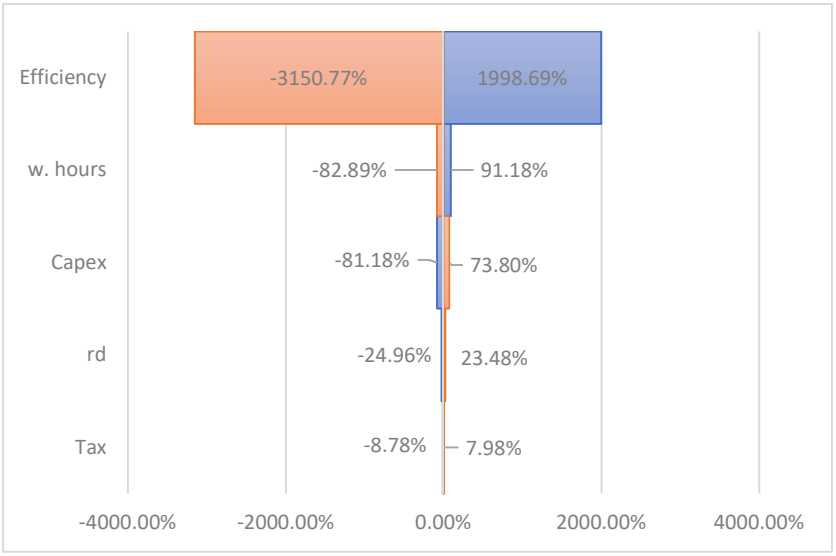

Figure 5.4 – Tornado diagram for NPV of modified electrolyzer (5% of Pt)

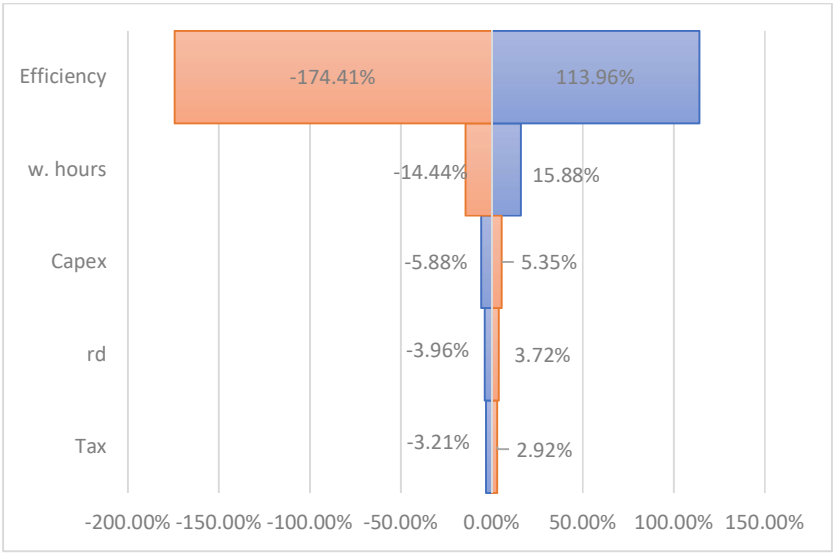

Figure 5.5 – Tornado diagram for NPV of modified electrolyzer (10% of Pt)

5.1 Methane price changing

At the moment, electrolysis is far inferior to steam methane reforming. Although a membraneless electrolyzer is not the most efficient electrolyzer, we can calculate at what price of methane membraneless electrolysis will become equally cost-effective as steam methane reforming.

Numerically, it was found that with 2.255 times increase of the calculated price (from 20 to 45.1 €/MWh, price for 2018 [19]), the NPV of steam methane reforming would decrease to the level of membraneless electrolysis.

Table 5.1.1 – Economic model for steam methane reforming for methane price increase

	0	1	2	3	4	5	6	7	8	9	10
Capex	-506										
Depr.		-51	-51	-51	-51	-51	-51	-51	-51	-51	-51
Opex		-317	-317	-317	-317	-317	-317	-317	-317	-317	-317
Rev.		506	506	506	506	506	506	506	506	506	506
EBT	0	138	138	138	138	138	138	138	138	138	138
EAT	0	108	108	108	108	108	108	108	108	108	108
CF	-506	158	158	158	158	158	158	158	158	158	158
DCF	-506	151	144	138	131	125	119	114	109	104	99
CDCF	-506	-355	-211	-73	58	183	302	416	525	629	728

Table 5.1.2 – Economical parameters comparison

	Steam methane reforming	Membraneless electrolysis
NPV, $	727.31	727.46
EAA, $	93.46	93.48

However, this situation with prices is not actual. Present (18.05.2022) gas price is 94.18 €/MWh [23], average electricity price for business is 0.096 $/kWh [24], carbon tax for Germany 29 $/$t_{CO2}$ [25].

Table 5.1.2 – Economical parameters comparison for actual prices

	Steam methane reforming	Membraneless electrolysis
NPV, $	-1302.13	-31.43
EAA, $	-167.32	-4.04

Right now, it is more profitable to produce hydrogen from electrolysis not steam methane reforming (however, both projects are non-efficient for selected discount rate). However, hydrogen must increase its market price as well, but, right now, no accurate data for May available.

Also, it was found that has prices should fall by 32.98% in order to make NPVs equal. Tables 5.1.3-5.1.5 present economical models for current prices and decrease of gas price.

Table 5.1.3 – Economic model for steam methane reforming for actual prices and gas price fall

	0	1	2	3	4	5	6	7	8	9	10
Capex	-506										
Depr.		-51	-51	-51	-51	-51	-51	-51	-51	-51	-51
Opex		-442	-442	-442	-442	-442	-442	-442	-442	-442	-442
Rev.		506	506	506	506	506	506	506	506	506	506
EBT	0	13	13	13	13	13	13	13	13	13	13
EAT	0	10	10	10	10	10	10	10	10	10	10
CF	-506	61	61	61	61	61	61	61	61	61	61
DCF	-506	58	55	53	50	48	46	44	42	40	38
CDCF	-506	-448	-393	-340	-290	-242	-196	-152	-110	-70	-32

Table 5.1.4 – Economic model for membraneless electrolysis for actual prices and gas price fall

	0	1	2	3	4	5	6	7	8	9	10
Capex	-373										
Depr.		-37	-37	-37	-37	-37	-37	-37	-37	-37	-37
Opex		-460	-460	-460	-460	-460	-460	-460	-460	-460	-460
Rev.		506	506	506	506	506	506	506	506	506	506
EBT	0	8	8	8	8	8	8	8	8	8	8
EAT	0	7	7	7	7	7	7	7	7	7	7
CF	-373	44	44	44	44	44	44	44	44	44	44
DCF	-373	42	40	38	36	35	33	31	30	29	27
CDCF	-373	-331	-291	-253	-217	-182	-149	-118	-88	-59	-32

Table 5.1.5 – Economical parameters for actual prices and gas price fall

	Steam methane reforming	Membraneless electrolysis
NPV, $	-31.43	-31.43
EAA, $	-4.04	-4.04

5.1 Sensitivity analysis conclusion

Tornado charts were made for NPV of all 5 projects with 10 % change of all parameters.

For steam methane reforming, the number of operating hours of the plant (and hence the amount of hydrogen produced) was most important. The consumption of electricity with this technology is small, so the electrical efficiency was the least significant.

For membraneless electrolysis both modified and traditional, the most crucial is efficiency (that is why PEM electrolysis is commercial used). Although modified pots have shown improvement in economic parameters, the only difference between modified pots and conventional pots is that changing other parameters affects all pots equally.

Relative economic efficiency of hydrogen production strongly depends on natural gas prices. In 2018, 2.255 times increase of gas price would make economically equal production of hydrogen via electrolysis and steam methane reforming.

Conclusion

In this work, an analysis of cubic tungsten carbide was performed. Methods for its possible synthesis were considered, and the plasma dynamic synthesis method used was described in more detail.

Tungsten carbide itself turned out to be an absolutely inefficient material: its electrocatalytic properties were much lower than the platinum sample. The introduction of a small fraction of platinum significantly increased the efficiency of the electrode, bringing it closer to the traditional one.

The sample with 10% platinum content proved to be the most promising: its NPV was the highest. This means that, probably, we can achieve better results by further increasing the platinum content of the electrode, for example, to 15%. It is also possible to use tungsten carbide not as a substitute for platinum, but as its co-catalyst, increasing the electrolysis efficiency, but his assumption requires further study.

However, at the moment, the obtained tungsten carbide does not have sufficient efficiency for its successful use in the commercial field. Its NPV is inferior to traditional membraneless hydrogen electrolysis: the reduction in capital costs does not cover the operating costs increased by lost process efficiency. In the future, it is possible to increase the purity of the material and, therefore, the efficiency, but at this stage its use is not advisable.

A sensitivity analysis compared 5 projects for the production and sale of hydrogen: steam methane reforming, membraneless electrolysis and three membraneless electrolysis with modified electrodes (1, 5, 10% platinum).

Most important for electrolysis projects was efficiency: the only resource for it is electricity that is why it is crucial. A 10% increase in efficiency made 2 projects cost effective. Steam methane reforming has little effect on its electrical efficiency, so the most important parameter was the number of working hours (and, of course, the scale of production).

An analysis was made sensitive to changes in the price of methane. For 2018 prices, a price increase of 2.255 times was enough for the steam methane reforming and membraneless electrolysis to be equally effective (considering that, moreover, membraneless electrolysis is not yet the most efficient type of electrolysis).

Currently (2022), green hydrogen production appears to be more efficient than gray hydrogen due to high natural gas prices. The price needs to fall by about a third to make hydrogen production via methane efficient again.

Overall, cubic tungsten carbide as a catalyst remains a promising technology for further development, as prices for platinum catalysts may increase in the future.

References

[1] A. P. Ilyin, O. B. Nazarenko, and D. V. Tikhonov, "Sintez karbidov metallov elektricheskim vzryvom provodnikov," *Vestnik nauki Sibiri*, 2012, Accessed: Mar. 13, 2021. [Online]. Available: https://cyberleninka.ru/article/n/sintez-karbidov-metallov-elektricheskim-vzryvom-provodnikov

[2] D. V. Onishchenko and V. P. Reva, "Polucheniye nanoporoshka karbida volframa metodom mekhanicheskoy aktivatsii," *Fizika i khimiya obrabotki materialov*, 2011, Accessed: Mar. 13, 2021. [Online]. Available: https://www.elibrary.ru/item.asp?id=16332744&

[3] R. Koc and S. K. Kodambaka, "Tungsten carbide (WC) synthesis from novel precursors," *J Eur Ceram Soc*, 2000, Accessed: Mar. 22, 2021. [Online]. Available: https://www.sciencedirect.com/science/article/abs/pii/S0955221900000388

[4] T. Ryu, H. Y. Sohn, K. S. Hwang, and Z. Z. Fang, "Plasma synthesis of tungsten carbide and cobalt nanocomposite powder," *Journal of Alloys and Compounds*, vol. 481, no. 1–2, pp. 274–277, Jul. 2009, doi: 10.1016/j.jallcom.2009.03.134.

[5] S. Tanaka, I. Bataev, H. Oda, and K. Hokamoto, "Synthesis of metastable cubic tungsten carbides by electrical explosion of tungsten wire in liquid paraffin," *Advanced Powder Technology*, vol. 29, no. 10, pp. 2447–2455, Oct. 2018, doi: 10.1016/j.apt.2018.06.025.

[6] Y. Lian *et al.*, "Solvent-Free Synthesis of Ultrafine Tungsten Carbide Nanoparticles-Decorated Carbon Nanosheets for Microwave Absorption," *Nano-Micro Letters*, vol. 12, no. 1, Jul. 2020, doi: 10.1007/s40820-020-00491-5.

[7] G.-L. Tan and X.-J. Wu, "Mechanochemical synthesis of nanocrystalline tungsten carbide powders," *Zhejiang University*, 1998, doi: 10.1179/pom.1998.41.4.300.

[8] A. A. Sivkov, A. Y. Pak, I. A. Rakhmatullin, and K. N. Shatrova, "Production of ultrafine tungsten carbide in a discharge plasma jet," *Nanotechnol Russ*, vol. 9, no. 11–12, pp. 682–687, Dec. 2014, doi: 10.1134/S1995078014060147.

[9] J. Kim, J. H. Jang, Y. H. Lee, and Y. U. Kwon, "Enhancement of electrocatalytic activity of platinum for hydrogen oxidation reaction by sonochemically synthesized WC1-x nanoparticles," *Journal of Power Sources*, vol. 193, no. 2, pp. 441–446, Sep. 2009, doi: 10.1016/j.jpowsour.2009.03.070.

[10] I. Shanenkov *et al.*, "Composite material WC1-x@C as a noble-metal-economic material for hydrogen evolution reaction," *Journal of Alloys and Compounds*, vol. 834, Sep. 2020, doi: 10.1016/j.jallcom.2020.155116.

[11] T. Christen and M. W. Carlen, "Theory of Ragone plots," *Journal of Power Sources*, vol. 91, pp. 210–216, 2000, doi: 10.1016/S0378-7753(00)00474-2.

[12] S. Koohi-Fayegh and M. A. Rosen, "A review of energy storage types, applications and recent developments," *Journal of Energy Storage*, vol. 27. Elsevier Ltd, Feb. 01, 2020. doi: 10.1016/j.est.2019.101047.

[13] D. v. Esposito, "Membraneless Electrolyzers for Low-Cost Hydrogen Production in a Renewable Energy Future," *Joule*, vol. 1, no. 4. Cell Press, pp. 651–658, Dec. 20, 2017. doi: 10.1016/j.joule.2017.07.003.

[14] J. T. Davis, “Membraneless Electrolyzers for Solar Fuels Production,” 2019.

[15] A. Manzotti, E. Quattrocchi, A. Curcio, S. C. T. Kwok, M. Santarelli, and F. Ciucci, “Membraneless electrolyzers for the production of low-cost, high-purity green hydrogen: A techno-economic analysis,” *Energy Conversion and Management*, vol. 254, Feb. 2022, doi: 10.1016/j.enconman.2021.115156.

[16] “Suisse Gold - Precious Metal Dealers.” https://www.suissegold.eu/en/charts/platinum (accessed Feb. 26, 2022).

[17] “Manufactures, Suppliers & Products in China.” https://www.made-in-china.com/products-search/hot-china-products/pure_tungsten_price.html (accessed Feb. 26, 2022).

[18] “Google search: Euro to dollar exchange.” https://www.google.com/search?client=opera&q=euro+to+dollar+exchange&sourceid=opera&ie=UTF-8&oe=UTF-8 (accessed Feb. 26, 2022).

[19] T. Keipi, H. Tolvanen, and J. Konttinen, “Economic analysis of hydrogen production by methane thermal decomposition: Comparison to competing technologies,” *Energy Conversion and Management*, vol. 159, pp. 264–273, Mar. 2018, doi: 10.1016/j.enconman.2017.12.063.

[20] “The Hydrogen and Fuel Cell Information System.” http://www.h2data.de (accessed Apr. 15, 2022).

[21] “Hydrogen cost and sales prices,” 2020. https://www.h2v.eu/analysis/statistics/financing/hydrogen-cost-and-sales-prices (accessed May 08, 2022).

[22] “Corporate Income Tax Rates in Europe,” 2022. https://taxfoundation.org/corporate-tax-rates-europe-2022/ (accessed May 08, 2022).

[23] “EU Natural gas 2022.” https://tradingeconomics.com/commodity/eu-natural-gas (accessed May 18, 2022).

[24] “Czech Republic electricity prices.” https://www.globalpetrolprices.com/Czech-Republic/electricity_prices/#:~:text=Czech%20Republic%2C%20September%202021%3A%20The,of%20power%2C%20distribution%20and%20taxes. (accessed May 18, 2022).

[25] “Carbon Pricing Dashboard.” https://carbonpricingdashboard.worldbank.org/map_data (accessed May 18, 2022).

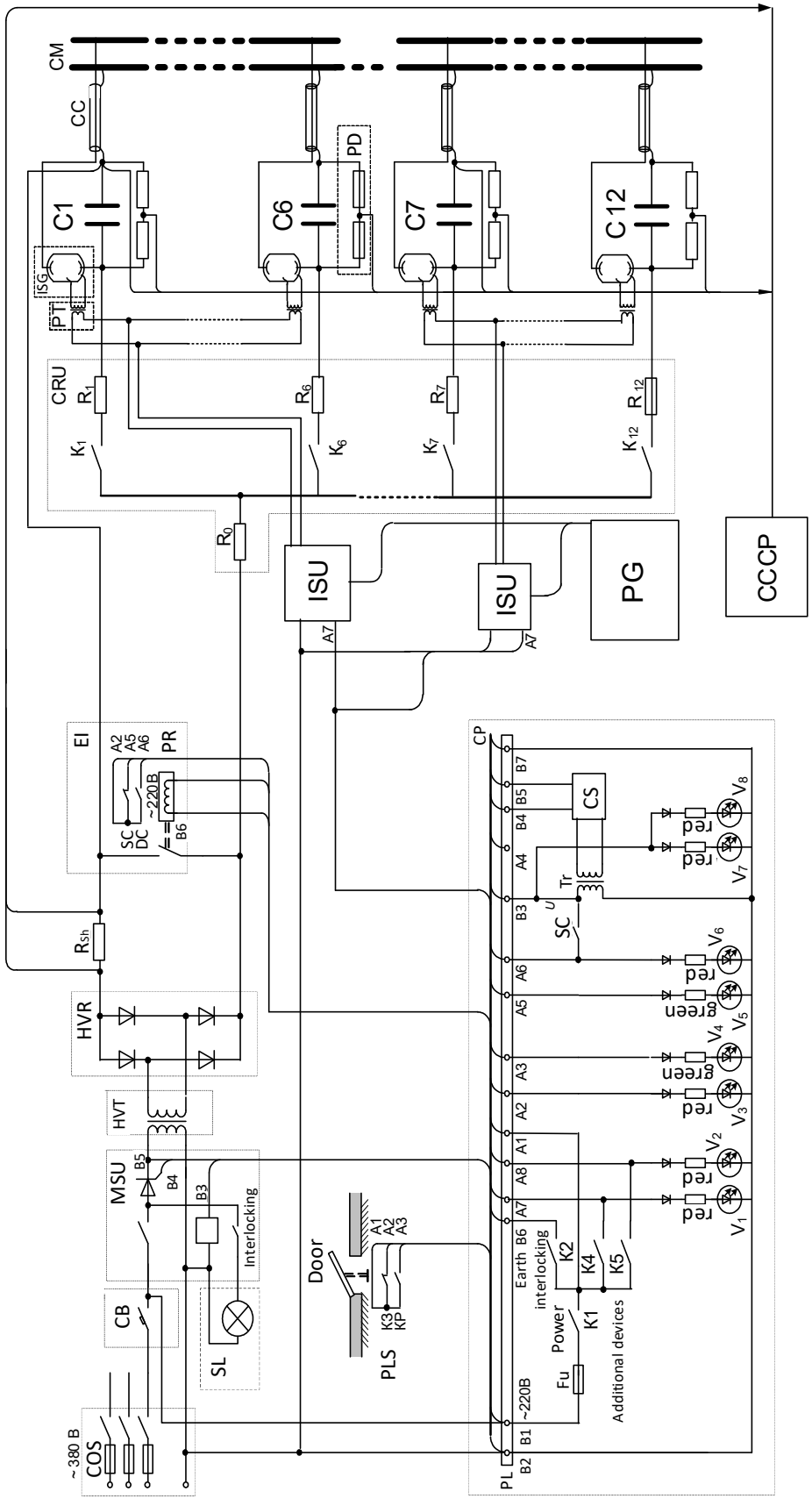

Figure 1 – CMPA electrical scheme